Biomaterials 31 (2010) 7266–7274

Contents lists available at ScienceDirect

Biomaterials

journal homepage: www.elsevier.com/locate/biomaterials

Self assembled bi-functional peptide hydrogels with biomineralization-directing peptides

Mustafa Gungormus [a], Monica Branco [b], Hanson Fong [a], Joel P. Schneider [b], Candan Tamerler [a], Mehmet Sarikaya [a,*]

[a] Materials Science and Engineering, University of Washington, Seattle, WA, USA
[b] Chemical Biology Laboratory, Center for Cancer Research, National Cancer Institute-Frederick, Frederick, MD, USA

ARTICLE INFO

Article history:
Received 15 April 2010
Accepted 1 June 2010
Available online 29 June 2010

Keywords:
Biomineralization
Biomimetic material
Peptide
Hydrogel
Scaffold
Hydroxyapatite

ABSTRACT

A peptide-based hydrogel has been designed that directs the formation of hydroxyapatite. MDG1, a twenty-seven residue peptide, undergoes triggered folding to form an unsymmetrical β-hairpin that self-assembles in response to an increase in solution ionic strength to yield a mechanically rigid, self supporting hydrogel. The C-terminal portion of MDG1 contains a heptapeptide (MLPHHGA) capable of directing the mineralization process. Circular dichroism spectroscopy indicates that the peptide folds and assembles to form a hydrogel network rich in β-sheet secondary structure. Oscillatory rheology indicates that the hydrogel is mechanically rigid ($G' \sim 2500$ Pa) before mineralization. In separate experiments, mineralization was induced both biochemically and with cementoblast cells. Mineralization-domain had little effect on the mechanical rigidity of the gel. SEM and EDXS show that MDG1 gels are capable of directing the formation of hydroxapatite. Control hydrogels, prepared by peptides either lacking the mineral-directing portion or reversing its sequence, indicated that the heptapeptide is necessary and its actions are sequence specific.

Published by Elsevier Ltd.

1. Introduction

A major ongoing challenge in the field of reconstructive and regenerative medicine is the successful repair or replacement of hard tissue, such as cartilage, bone, and dental tissues, which have been lost due to disease, congenital defects or trauma. Autograft tissue is considered as one of the best sources for the replacement of lost hard tissue. Its use, however, is limited due to difficulties in harvesting substantial amounts of autologous grafts with the appropriate shapes[1]. Allografts and xenografts of freeze-dried or de-mineralized hard tissue have also been utilized for repair; however major limitations exist for these materials, such as the risk of host immune response and, more importantly, the transfer of pathogens such as HIV and hepatitis viruses [2]. To overcome the inadequacies of current tissue repair and reconstruction strategies, a variety of tissue engineering approaches has been developed and expanded with a focus on utilizing synthetic tissue scaffolds to replace or regenerate the lost tissue.

Some of the most commonly investigated materials for possible hard tissue scaffolds include natural materials, such as cornstarch-based polymers [3], chitosan [4], collagen [5], natural calcium phosphates [6–8], synthetic materials, such as calcium phosphates of inorganic origin [9,10] and synthetic inorganic polymers [11,12]. Many of these scaffolds have been designed to be mimics of bone, e.g., possessing similar mechanical properties of the hard tissue. The complexity and highly hierarchical structure of hard tissues, however, often require tissue scaffolds that provide an architectural support for the cells, as well as influence and guide the structural properties of the newly formed mineral phase. Soluble extracellular matrix (ECM) proteins play an important role in this process [13–15]. Therefore, many of the key proteins thought to regulate bone development have been incorporated within tissue scaffolds. For example, bone morphogenetic proteins (BMPs), Arginine–Glycine–Aspartic acid (RGD) peptides, and P15 peptides [13,16,17] are amongst the most widely used bioactive molecules to develop biomimetic tissue scaffolds. Although there are many exciting examples, the lack of knowledge on both the function and the temporal and spatial distribution of the proteins involved in biological mineralization have largely limited the successful use of these proteins in tissue engineering. An alternate approach is to

* Corresponding author. GEMSEC, Genetically Engineered Materials Science and Engineering Center, Department of Materials Science & Engineering, 327 Roberts Hall, University of Washington, Seattle, WA 98195, USA.
E-mail addresses: musgun@u.washington.edu (M. Gungormus), monica.branco@nih.gov (M. Branco), hfong@u.washington.edu (H. Fong), Joel.Schneider@nih.gov (J.P. Schneider), Candan@u.washington.edu (C. Tamerler), sarikaya@u.washington.edu (M. Sarikaya).

0142-9612/$ – see front matter Published by Elsevier Ltd.
doi:10.1016/j.biomaterials.2010.06.010

incorporate small peptides within a material matrix that can guide biomineralization. Our labs are developing genetically engineered peptides that selectively bind to inorganics (GEPIs). The GEPIs are selected by exposing a pool of random amino acid sequences, displayed on the surface of a host organism (e.g. bacteriophage or bacteria) [18,19] to a target inorganic solid substrate and identifying the strongly binding sequences [20]. It has been shown that GEPIs can bind to solid substrates specifically and significantly influence the inorganic material formation processes [21–26].

For many implantable hard materials, regardless of how similar the mechanical and physiochemical properties of designed scaffold are to the living bone, when clinical application is considered, the many advantages offered by these materials can be lost if the scaffold cannot be implanted correctly at the defect site. Poor tissue integration due to improper apposition at the site of implantation is a major failure mechanism of many tissue engineering materials. Thus, an *in situ* forming scaffold, where the three-dimensional matrix is formed at the defect site, would be advantageous. These materials eliminate the complications originating from the prefabrication process and improve the physical contact between the scaffold and the surrounding tissue. These materials can be introduced to the wound bed in a minimally invasive manner *via* a syringe. For example, the synthetic polymer, poly(methyl methacrylate) (PMMA), is a widely used *in situ* forming material in clinical orthopedics. Although PMMA has been shown to be very successful in many applications, its use, however, is limited due to the exothermic polymerization reaction that occurs during material formation, usually leading to the necrosis of the surrounding tissue [27]. Moreover, the non-degradable nature of PMMA poses a risk for foreign body response and may slow down the healing of the hard tissue. Synthetic polymers, such as poly(propylene fumarate) [28] and polyanhydride [29], have also been utilized as *in situ* forming scaffolds. These polymers are cytocompatible and, hence, partially eliminate the risk of foreign body response, but their utility is curtailed due to the highly cross-linked nature of the network formed, posing limitations in maintaining cell viability. An attractive alternative for *in situ* forming tissue scaffolds would be hydrogels formed from self-assembling materials such as amphiphilic peptides or proteins [30–43]. Peptide hydrogels enable formation of scaffold materials that mechanically resemble the native ECM and can be formed at the site of implantation without the use of harsh chemical cross-linking agents or the presence of adverse assembling reactions that can affect the surrounding tissues.

In this work, we describe the development of an *in situ* forming, self-assembling peptide hydrogel that is capable of directing the mineralization of calcium phosphate. The peptide, MDG1 (Mineral Directing Gelator), undergoes triggered intra-molecular folding into a conformation that subsequently self-assembles to form a fibrillar network where a mineral-directing GEPI sequence is displayed from the fibrils that constitute the gel, Fig. 1. The ability to form three-dimensional networks that carry an inherent functionality makes these hybrid peptides attractive candidates for use in tissue engineering applications and suitable models for developing, multifunctional structures for nano-technological applications.

2. Materials and methods

2.1. Peptide synthesis and purification

Peptides were synthesized on RINK amide resin via an automated ABI 433A peptide synthesizer employing standard Fmoc-protocol and HCTU activation. The resulting resin-bound peptides were cleaved and side-chain deprotected for 2 h using a TFA: thioanisole: ethanedithiol: anisole (90:5:3:2) cocktail. Filtration followed by ether precipitation yielded crude peptides that were purified by RP-HPLC using a Vydac C18 peptide/protein column [44] Analytical HPLC profiles and ESI (+) mass spectroscopy spectrum of the pure peptides are provided in the Supporting Information.

2.2. Circular dichroism

Circular dichroism experiments were performed on a Jasco J-810 spectropolarimeter. Stock 300 μM solutions of each peptide were prepared in chilled pH 7.4, 25 mM Tris buffer. 150 μL of the peptide stock was placed in a 1 mm quartz cell. To the same cell, 150 μL of chilled pH 7.4, 25 mM Tris buffer containing 48 mM $CaCl_2$ and 28.8 mM β-glycerophosphate (β-GP) was added. The quartz cell was gently mixed by cell inversion to yield the final peptide solution (150 μM peptide, 25 mM Tris, 24 mM $CaCl_2$, and 14.4 mM β-GP). The cell was immediately placed in the CD cell holder pre-equilibrated at 5 °C. Temperature dependent wavelength spectra were collected every 5 °C up to a maximum temperature of 80 °C with a 10 min equilibration time at each temperature. The concentration of the peptide solutions were determined by UV–vis absorbance at 220 nm ($\varepsilon = 21{,}263\ cm^{-1}\ m^{-1}$ for MDG1 and cMDG1, $\varepsilon = 15{,}750\ cm^{-1}\ m^{-1}$ for MAX8). Mean residue ellipticity [θ] was calculated from the equation, $[\theta] = \theta_{obs}/(10 \times l \times c \times r)$, where θ_{obs} is the measured ellipticity

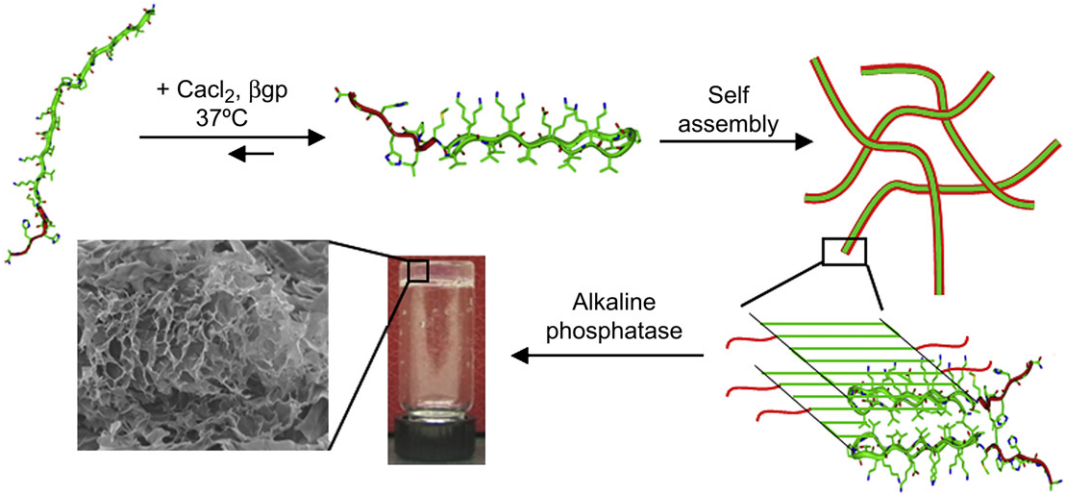

Fig. 1. Schematic representation of the folding, self-assembly, and resultant hydrogelation of MDG1, cMDG1, and MAX8 peptides. Sequences of the three peptides are shown.

(millidegrees), *l* is the length of the cell (centimeters), *c* is the concentration (molar), and *r* is the number of residues.

2.3. Dynamic oscillatory rheology

Oscillatory rheology experiments were performed on a Paar Physica MCR 500 rheometer using a 25 mm diameter stainless steel parallel plate geometry. For the 1 h rheological measurements, gels were prepared directly on the rheometer plate. To prepare 1 wt% hydrogels, peptide stock solutions were first prepared in glass vials by dissolving 3.5 mg of each peptide in 175 μL of chilled pH 7.4, 25 mM Tris buffer. To the stock solution, 175 μL of chilled Tris buffer (25 mM, pH 7.4) containing 48 mM $CaCl_2$ and 28.8 mM β-GP was added. Then, 300 μL of the stock solution was quickly added to the rheometer plate, which was pre-equilibrated at 5 °C. The parallel plate tool was then lowered to a gap height of 0.5 mm and the temperature was ramped linearly to 37 °C to initiate gelation. Initially, a dynamic time sweep was performed to measure the storage (G′) and loss (G″) modulus at a frequency of 6 rad/s and 0.2% strain as a function of time for an hour. A dynamic frequency sweep (0.1–100 rad/s at constant 0.2% strain) was then performed, followed by a dynamic strain sweep (0.1–1000% strain at constant 6 rad/s) for all samples to ensure the hydrogels were within the linear viscoelastic regime.

For the 24 h rheological measurements, gels were made in a 3.5 K molecular weight cut-off dialysis cassette (Pierce, USA) and then transferred to the rheometer plate for assessment. Peptide stock solutions were first prepared in glass vials by fully dissolving 6 mg of each peptide in 300 μL of sterile, chilled pH 7.4, 25 mM Tris buffer. To this solution, 300 μL of chilled Tris buffer (25 mM, pH 7.4) containing 48 mM $CaCl_2$ and 1.4×10^{-6} mg/mL alkaline phosphatase was then added. Then, 500 μL of the stock solution was degassed with continuous nitrogen flow and quickly added to the dialysis cassette. Control stock solutions were prepared with Tris $CaCl_2$ buffer containing no alkaline phosphatase. The dialysis cassettes containing the hydrogels were placed in an incubator equilibrated at 37 °C. Two hours after gel preparation, the dialysis cassettes were immersed in a 500 mL solution of pH 7.4, 25 mM Tris buffer containing 24 mM $CaCl_2$ and 14.4 mM β-GP. Hydrogels were placed in an incubator equilibrated at 37 °C overnight. After 24 h, the gels were removed from the dialysis cassettes and the gels were transferred to the rheometer plate, which was equilibrated at 37 °C. The parallel plate tool was then lowered to a gap height of 0.5 mm. A dynamic time sweep was performed for 15 min to ensure that G′ and G″ reached a plateau, followed by a dynamic frequency sweep and a dynamic strain sweep for all samples, with the same parameters as the 1 h rheology studies.

2.4. Hydrogelation and solution mineralization

Mineralization experiments were performed in a 3.5 K molecular weight cut-off dialysis cassette (Pierce, USA) using an Alkaline Phosphatase (AP) mediated mineralization model that mimics matrix vesicle mineralization. A mineralization solution was prepared by diluting stock solutions of $CaCl_2$ and AP to final concentrations of 24 mM and 1.4×10^{-6} mg/mL respectively, in 200 μL of pH 7.4 Tris buffer. 2 mg of peptide was dissolved in this mineralization solution. The solutions were degassed with continuous nitrogen flow and injected into the dialysis cassette. The solution was allowed to gelate at 37 °C in a humidified chamber for 2 h. After gelation was complete, the cassette was immersed into a 14.4 mM β-glycerophosphate solution in the same buffer and allowed to mineralize for an additional 22 h. The mineralization took place through the hydrolysis of β-glycerophosphate by the AP entrapped in the gel and the reaction of the released inorganic phosphate group with the calcium.

2.5. Cell culture

An immortalized mouse cementoblast cell line, (OCCM-30), was maintained in DMEM supplemented with 10% FBS, 100 U/mL penicillin, and 100 μg/mL streptomycin. Cells were encapsulated within the hydrogel in the following manner. First, MDG1 and MAX8 were dissolved separately at a concentration of 1 wt% in water. Then an equal volume of serum free DMEM, containing 2×10^4 OCCM-30 cells, 100 μg/mL ascorbic acid and 40 mM β-GP was added to the peptide solution, resulting in a 0.5 wt% hydrogel with 50 μg/mL ascorbic acid and 20 mM β-GP. The mixture was allowed to gel in 96 well plates for 10 min at 37 °C. DMEM containing 1%FBS was then added on top of the gels. The cells were cultured in the gels for 9 days and fresh media containing 1%FBS, 50 μg/mL ascorbic acid and 20 mM β-GP was added every other day to the top of the gels.

An SYTO 9/Propidium iodide based live dead assay (Invitrogen, USA), where only the dead cells are stained with propidium iodide and gave red fluorescence, was used to test the viability of the cells in the hydrogel. The cells were encapsulated as described below and at the end of 3 days, a 1:1 mixture of SYTO 9/Propidium iodide was added on top of the gels and incubated for 30 min. The gels were then washed three times with serum free DMEM and imaged using a TE 300L microscope (Nikon, Japan) with the appropriate filters. A z-series of 10 images with 35 μm step sizes were taken and the images were reconstructed using MetaMorph Imaging System version 6.2 (Photometrics UK Ltd., UK, formerly Universal Imaging Co., USA). The viable and the dead cells were counted using ImageJ image processing software (NIH, USA).

2.6. Electron microscopy analysis

At the conclusion of the mineralization studies (24 h for solution mineralization and 9 days for cell culture mineralization), the hydrogels were immersed into liquid nitrogen and lyophilized. The lyophilized gels were kept desiccated at −20 °C until analyzed by microscopy. For scanning electron microscopy (SEM), the lyophilized gels were placed on a carbon tape and coated with platinum prior to microscopy. SEM imaging and energy dispersive X-ray spectroscopy (EDXS) were performed using a JSM 7000F (JEOL) SEM at 10 kV in secondary electron imaging mode. For transmission electron microscopy (TEM), the lyophilized gels were mounted on double folding copper TEM grids. TEM imaging and electron diffraction were performed using an EMS 420 T TEM at 120 kV (FEI, Inc., USA; formerly Philips, The Netherlands).

2.7. X-ray diffraction analysis

X-ray diffraction (XRD) measurements were performed to identify the final phase of the mineral deposited on the gels. The gel samples were collected by redissolving the lyophilized gel-mineral composite in distilled water to solubilize the peptide matrix. The mineral component was isolated by centrifugation. Collected mineral was dried in vacuum at room temperature prior to the measurements. The measurements were performed on a D8 Focus model diffractometer employing CuKα radiation, 40 kV and 40 mA (Bruker, USA). Data were collected in the range of $2\theta = 3°$ to 60° using a 0.05° step size and 1 s/step scan speed. The XRD spectra were analyzed using Jade software version 8.5 (Materials Data Inc, USA).

3. Results and discussion

3.1. Peptide material design

MDG1 is a twenty-seven residue peptide designed to undergo triggered intra-molecular folding and subsequent self-assembly to form a fibrillar network affording a mechanically rigid gel, Fig. 1. When dissolved in pH buffered water at low ionic strength, the peptide remains unfolded due to unfavorable electrostatic interactions between residue side chains. When a solution containing $CaCl_2$ and β-GP is added, these interactions are screened and the peptide is able to fold. The N-terminal twenty residues of MDG1 are designed to adopt an amphiphilic β-hairpin when the peptide folds. This N-terminal portion contains two β-strands connected by a four residue sequence (-V^{D}PPT-) known to adopt a type II' β-turn [45]. The β-strands are composed of alternating hydrophobic and hydrophilic residues that give the hairpin its amphiphilic character in the folded state. The N-terminal portion of MDG1 has been reported in the literature and studied extensively (e.g. MAX8: VKVKVKVKV^{D}PPTKVEVKVKV-$CONH_2$) [46,47]. MAX8 hairpins readily self-assemble affording a fibrillar network where each fibril is composed of a bilayer of hairpins that have self-assembled laterally via intermolecular hydrogen bond formation along the long axis of a given fibril, Fig. 1 [47–49]. Hydrogels formed from MAX8 are mechanically rigid, viscoelastic materials that are cytocompatible. The C-terminal seven residues of MDG1 (MLPHHGA) were incorporated at the hairpin terminus so that this sequence could be displayed from the fibril surface and direct mineralization. This small peptide had been reported in the literature and named HABP1 (MLPHHGA) [50]. It was identified *via* phage display and had been shown to control calcium phosphate mineral formation in solution. Specifically, HABP1 slows the mineralization rate and accelerates the transformation of amorphous calcium phosphate (ACP) into crystalline octacalcium phosphate (OCP) during mineralization. This results in the formation of elongated, plate-like particles. The full length peptide, MDG1 should fold and assemble, forming hydrogels capable of directing calcium phosphate mineralization.

In addition to the MDG1 hydrogel, two control hydrogels were prepared and studied. The first control gel is formed by the self-assembling peptide, cMDG1. This peptide is identical to the parent

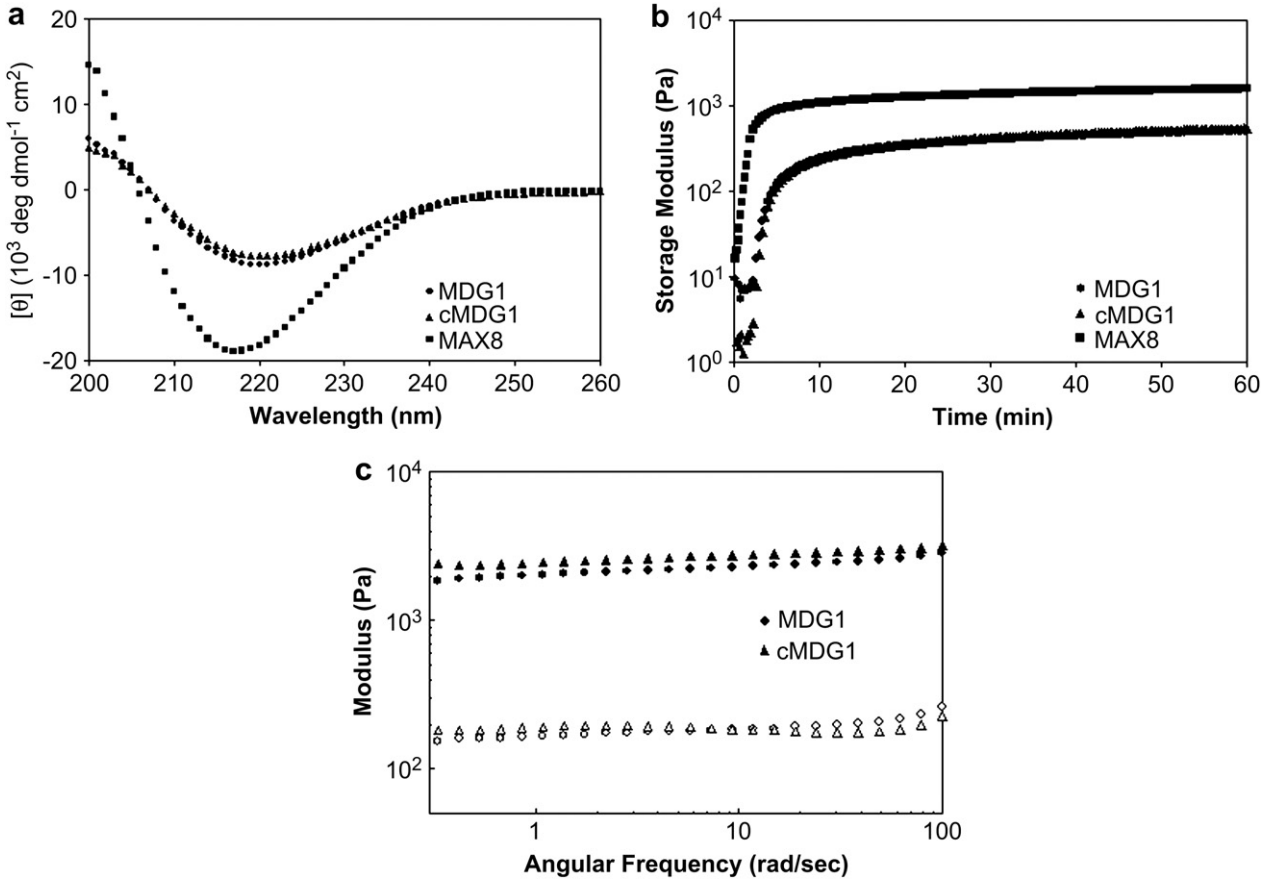

Fig. 2. (a) CD wavelength spectra of 150 μM of MDG1, cMDG1, and MAX8 in pH 7.4 Tris–HCl buffer, 24 mM $CaCl_2$, and 14.4 mM β-glycerophosphate at 37 °C. (b) Dynamic oscillatory rheology of 1 wt% peptides in pH 7.4 Tris–HCl buffer, 24 mM $CaCl_2$, and 14.4 mM β-glycerophosphate formed at 37 °C. (c) Dynamic frequency sweep of 1 wt% peptides after 24 h incubation at 37 °C. Hydrogels are prepared with pH 7.4 Tris–HCl buffer containing 24 mM $CaCl_2$ directly in a dialysis cassette that is then incubated for 2 h at 37 °C. The cassette is then immersed in a pH 7.4 Tris–HCl buffer containing 24 mM $CaCl_2$ and 14.4 mM β-glycerophosphate for an additional 22 h at 37 °C.

peptide except that the sequence of the seven C-terminal residues is reversed. cMDG1 examines the role that sequence specificity and amino acid composition play in directing mineral deposition. If sequence specific interactions are made between the C-terminal sequence of MDG1 and inorganic species during mineralization, distinct mineral morphology and type should be observed as compared to mineral deposits formed in hydrogels comprised of the control peptide (cMDG1). If there is little difference in the type of mineral deposited, this would suggest that sequence specific interactions are largely not at play and that non-specific interactions, such as gross electrostatics, may be more important. This would suggest that amino acid composition, rather than sequence specificity, is the more relevant design parameter. The second control hydrogel is formed by the peptide MAX8, which lacks the mineral-directing portion. This control gel was used to determine if the fibrillar scaffold alone could direct mineralization. In addition, the MAX8 control was used to assess what effect adding a C-terminal sequence to an otherwise symmetrical β-hairpin had on peptide folding, self-assembly and the rheological properties of the resultant hydrogel.

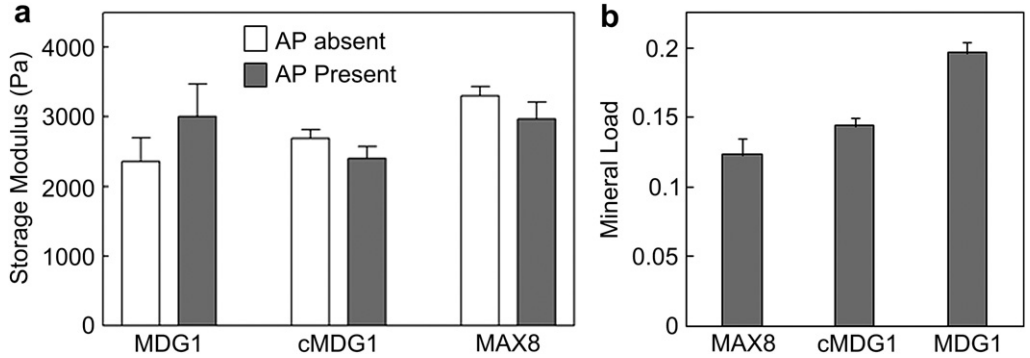

Fig. 3. (a) Average storage modulus values (6 rad/s) of 1 wt% gels after 24 h incubation at 37 °C in the absence or presence of alkaline phosphatase, which was used to promote mineraliztion. (b) Mineral load of the gels after 24 h of mineralization.

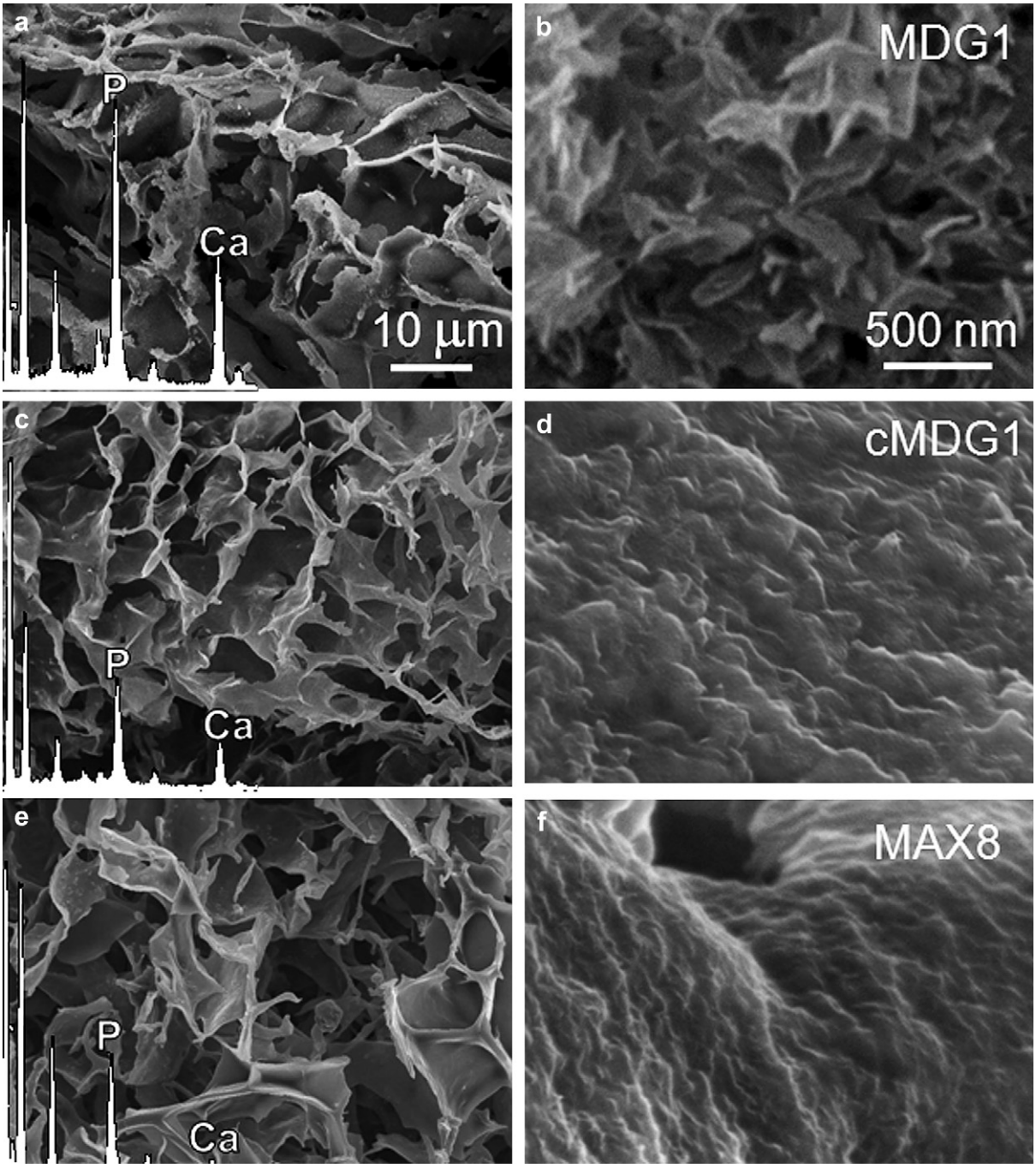

Fig. 4. SEM micrographs and corresponding EDXS spectra of lyophilized MDG1 (a), cMDG1 (c), and MAX8 (e) gels after 24 h mineralization. The morphological differences among the deposited minerals are observable at higher magnifications in panels b, d and f, respectively.

3.2. Triggered folding, self-assembly and hydrogelation

The peptide construct MDG1 was designed to undergo triggered folding and self-assembly resulting in the formation of a mechanically rigid hydrogel in the presence of $CaCl_2$ and β-GP. Mineralization within the gel is possible when Alkaline Phosphatase is added to cleave β-GP, liberating phosphate, which then participates in the formation of calcium phosphate mineral. Circular dichroism (CD) spectroscopy was used to follow the folding and subsequent self-assembly of MDG1 at pH 7.4, 37 °C in response to the addition of $CaCl_2$ and β-GP. These salts screen unfavorable electrostatic side-chain interactions that normally inhibit peptide folding. Fig. 2a shows wavelength spectra for MDG1, cMDG1, and MAX8 peptide solutions after folding had been initiated. Low concentrations (150 μM) of peptide were used for the CD studies to limit scattering and aid data acquisition; at this concentration, the peptides do not form gels but still fold and assemble into soluble β-sheet-rich fibrils whose secondary structure can be easily monitored. All three peptides display spectra characteristic of β-sheet structure with minima at ~217 nm. The spectra of MDG1 and cMDG1 are nearly identical indicating that the manner in which the GEPI, mineral-directing sequence is attached is inconsequential with respect to the ability of the hairpin portion to fold and assemble. Also evident is the fact that the absolute value of the mean residue ellipticity at

217 nm for the MAX8 control peptide is greater. This indicates that the seven C-terminal residues of MDG1 and cMDG1 do not contribute to the β-sheet signal. Previous CD studies of the hepta-peptide (MLPHHGA) alone indicate that this peptide exists in an equilibrium of polyproline and random coil conformations [50]. Taken together, the CD data suggests that MDG1 and cMDG1 fold, affording hairpins that assemble into β-sheet-rich fibrils that display structurally flexible mineral-directing motifs as depicted in Fig. 1.

Fig. 2b shows dynamic oscillatory shear rheology time sweep experiments that monitor the evolution of the storage modulus (G′, a measure of a material's elastic response to applied strain after peptide folding, self-assembly and subsequent hydrogelation has been triggered. Rheology of the three peptides was performed at a peptide concentration of 1 wt % at pH 7.4 in 25 mM Tris buffer containing 24 mM $CaCl_2$ and 14.4 mM β-GP at 37 °C. Both MDG1 and cMDG1 form viscoelastic hydrogels within the first 10 min of the experiment ultimately yielding gels with storage moduli of 510 ± 10 Pa and 590 ± 100 Pa, respectively after 1 h. In comparison, the control peptide MAX8 lacking any C-terminal extension forms a much more rigid gel, more quickly, with a modulus of 1650 ± 150 Pa after 1 h. Taken together, this data suggests that the C-terminal extensions of MDG1 and cMDG1 decrease the rate of hydrogelation and reduce the mechanical rigidity of their respective hydrogels. The experiments in Fig. 2b involve forming the gels *in situ* directly in the rheometer and the gels are allowed to cure for only 1 h. Interestingly, when MDG1 and cMDG1 gels are incubated at 37 °C for 24 h, their rigidities increase to nearly 2500 Pa Fig. 2c shows frequency sweep data taken at 24 h; G′ values for MDG1 and cMDG1 have increased to 2400 ± 300 Pa and 2700 ± 100 Pa at a frequency of 6 rad/s, respectively and are an order of magnitude greater than the loss modulus (G″).

3.3. Biomineralization

The ability of the MDG1 hydrogel to promote and direct mineralization was probed by rheology, quantitative mineral load assessment, spectroscopy, microscopy and diffraction experiments. In the biomineralization experiments we used an enzyme-mediated mineralization model to mimic vertebrate biomineralization, where AP controls calcium phosphate formation by hydrolyzing organophosphate groups releasing inorganic phosphate. Here, therefore, our model consists of AP entrapped within the hydrogel in the presence of β-GP. Hydrogels used in the mineralization studies were prepared employing a dialysis cassette. Hydrogels were formed by initiating gelation with a solution of $CaCl_2$ containing alkaline phosphatase directly in the cassette. Gelation was allowed to proceed over 2 h and then the cassette was immersed in a bath that contained a buffered (pH 7.4) solution of β-GP and $CaCl_2$. Mineralization occurred as the β-GP diffused into the cassette and was cleaved by the enzyme. For all the peptide gels (MDG1, cMDG1 and MAX8), as mineralization takes place, the initially optically clear gels become opaque. No mineralization was observed in the immersion buffer indicating that all the calcium phosphate deposition took place within the hydrogel. Fig. 3a shows rheological data comparing mineralized and non-mineralized gels formed under identical conditions. The mechanical rigidity of MDG1 gels increased slightly after 24 h of mineralization. In comparison, the rigidities of both control peptides were affected little by the mineralization process. The measured mineral loads within each of the gels (Fig. 3b) show a similar trend. The MDG1 gel accommodates a slightly higher load than the control gels. The data in Fig. 3 indicate that all three peptide gels are capable of supporting mineralization and that the C-terminal, mineral-directing attachment has no effect on gross mineralization.

Next, studies were performed to assess whether or not the mineral-directing peptide attachment could control the crystal morphology and the phase of the deposited calcium phosphate mineral. Scanning electron microscopy (SEM) images of lyophilized peptide hydrogels after mineralization are displayed in Fig. 4a. With the understanding that the lyophilization treatment can influence material morphology, a highly porous structure with 10–15 μm pore sizes was the governing morphology observed for the MDG1, cMDG1 and MAX8 hydrogel networks. Energy dispersive X-ray spectroscopy (EDXS) analysis reveals that calcium phosphate mineralization took place in all three gels (Fig. 4a,c,e – insets). As expected, no calcium or phosphate was observed in the non-mineralized gels (data not shown). At higher magnification, morphological differences in the deposited mineral on MDG1 become evident, appearing more crystalline (Fig. 4b), suggesting that the C-terminal appendage (MLPHHGA) may be influencing mineral morphology. In contrast, a poorly crystalline mineral film was observed on the control cMDG1 and MAX8 hydrogels (Fig. 4d and f). Transmission electron microscopy (TEM) analysis further supports this assertion and shows distinct differences in the crystallinity of the deposited minerals within each of the peptide hydrogels, Fig. 5. Mineral deposited within the MDG1 gel was highly crystalline and elongated, resembling biological apatite. The average length of these crystals was 100 nm with an approximate aspect ratio of between 1:10–1:20. Selected area electron diffraction analysis confirmed the crystallinity of the particles. The mineral deposited within MDG1 showed a sharp 002 diffraction peak, indicating the thin plate-like nature of the crystals, and a broad diffraction band containing the 211, 112, and 300 triple diffraction peaks, which are characteristic to biological apatite (Fig. 5a – inset). Few individual particles were observed on the cMDG1 gel, which includes the reversed mineral-directing sequence, (Fig. 5b). In addition, the poor quality of these crystals

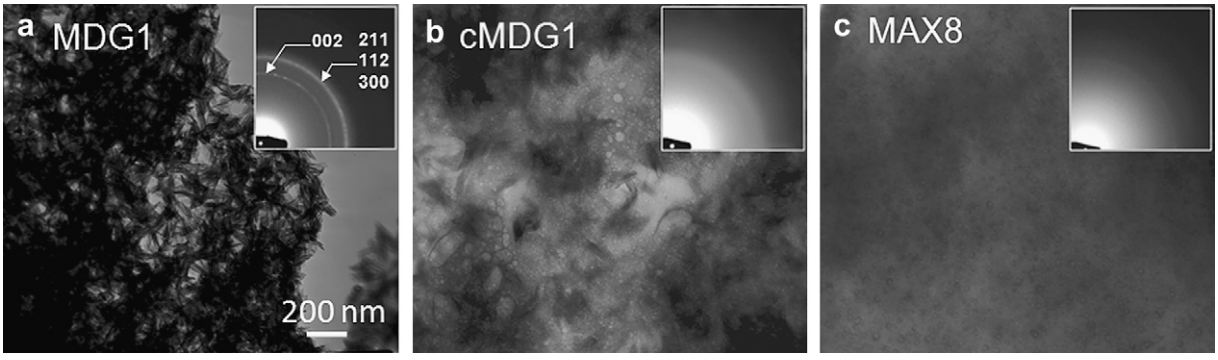

Fig. 5. TEM micrographs and the corresponding electron diffraction pattern (insets) of lyophilized MDG1 (a), cMDG1 (b), and MAX8 (c) gels after 24 h mineralization.

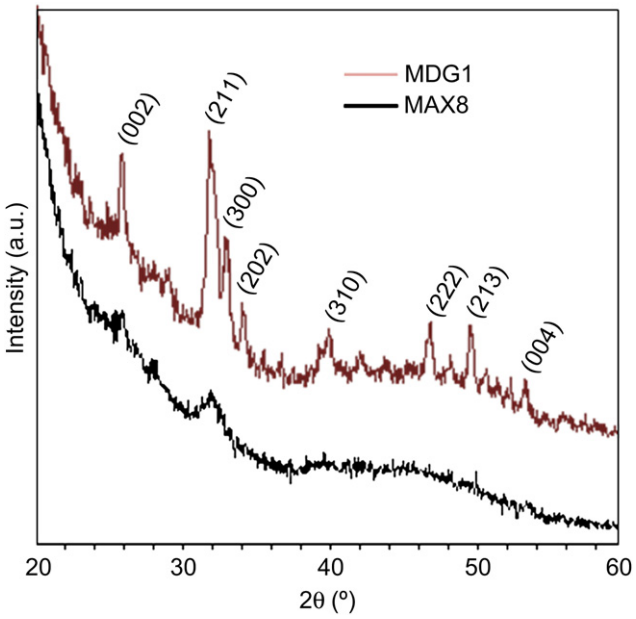

Fig. 6. XRD patterns of mineral deposited on MDG1 and MAX8 hydrogels.

resulted in highly diffused electron scattering (Fig. 5b – inset). Lastly, no individual particles were observed on the MAX8 gels, consistent with the fact that the mineral-directing sequence was not present.

Identification of the final calcium phosphate phase is often difficult by electron diffraction analysis alone because of the similar crystal structure of octacalcium phosphate (OCP) and hydroxyapatite (HA). One of the key diffraction effect, i.e., the characteristic OCP ring that corresponds to (100) ($d = 18.6$Å), is usually masked by the transmitted beam in the electron diffraction pattern. Therefore, X-ray diffraction (XRD) measurements were performed in addition to electron diffraction analysis to eliminate these uncertainties in phase identification. The results obtained from the XRD analyses were consistent with the morphological observations and the electron diffraction analyses obtained by TEM. The XRD pattern of the mineral deposited on MDG1 consisted of numerous sharp peaks indicative of crystalline HA, Fig. 6. The major peaks were observed at $2\theta = 31.8^\circ$ ($d = 2.81$Å) and 32.1° ($d = 2.78$Å) corresponding to (211) and (300) planes, respectively. In comparison, the mineral deposited on the MAX8 control yielded only a weak and broad peak at $2\theta = 31.8^\circ$ ($d = 2.81$Å) indicating a small amount of poorly crystalline HA. For both MDG1 and MAX8 gels, diffraction peaks corresponding to other crystalline phases were not observed. Taken together, the microscopy and the diffraction studies suggest that the fibril network alone can accommodate mineralization. However, the mineral-directing attachment can influence the morphology of the deposited mineral. In addition, the data also indicates that the peptide attachment must be displayed from the fibrils with sequence fidelity, suggesting that, here, sequence specific interactions with mineral components are being made to direct mineralization.

3.4. Cell viability and mineralization

The response of cells to the MDG1 matrix was assessed by monitoring mineralization induced by encapsulated cementoblasts. Cells were directly embedded in a 0.5 wt% MDG1 hydrogel by initiating peptide folding and self-assembly in the presence of cells (see Experimental Section). In this experiment, the DMEM media contained calcium and β-GP; viable cells should produce and secrete alkaline phosphatase to drive mineralization if the MDG1 hydrogel is cytocompatible. Upon 3 days of post encapsulation, cell viability assay shows that encapsulated cementoblasts were viable in the MDG1 matrix with 597 ± 25 live cells versus 157 ± 12 dead cells per 7.5×10^{-5} cm^3 (Fig. 7a). After 9 days of culture in the mineralizing conditions, SEM analysis indicates that the cells were capable of mineralizing the MDG1 fibril network. The energy dispersive x-ray spectroscopy (EDXS) results show clearly observable calcium phosphate peaks. The mineral deposited on the MDG1 fibrils appeared homogenous in its consistency in contrast to the characteristic large, isolated mineral nodules observed when cementoblasts are cultured on a 2D tissue culture plate in the absence of gel, Figure S1a. The mineral morphology, observed in the MDG1 hydrogels, is consistent with that produced by cementoblast cultures in 2D in the presence of the mineral-directing sequence (MLPHHGA) alone, Figure S1b. Previous studies show that this small sequence decreases the rate of mineralization resulting in a slow nucleation favored regime resulting in a homogeneous deposition of mineral instead of the rapid growth of isolated mineral nodules [50]. The data indicate the mineral-directing sequence can also function when directly appended to a material scaffold and does not affect the ability of cementoblasts to produce alkaline phosphatase which, in turn, directs mineralization.

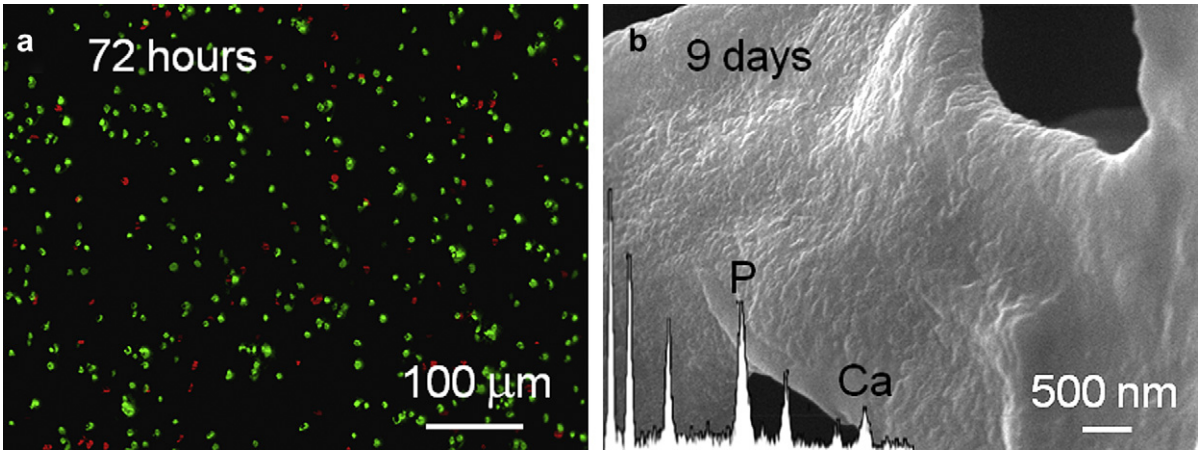

Fig. 7. (a) Live/dead cytotoxicity assay on cementoblast cells 3 days after encapsulation into the MDG1 matrix. Viable cells fluoresce green and the dead cells fluoresce red. (b) SEM micrographs of the MDG1 matrix mineralized by cementoblasts after 9 days. The inset shows the corresponding EDXS. (For interpretation of the reference to colour in this figure legend, the reader is referred to the web version of this article.)

4. Conclusion

In this study, we have designed, synthesized and studied the mineralization potential of a peptide-based hydrogel. The peptide, MDG1, undergoes triggered folding to form an unsymmetrical β-hairpin that self-assembles in response to an increase in solution ionic strength to yield a mechanically rigid, self supporting hydrogel. The C-terminal portion of MDG1 contains a heptapeptide capable of directing the mineralization process of calcium and phosphate to produce hydroxyapatite. The ability to form well defined three-dimensional networks that carry an inherent functionality makes these hybrid peptides attractive candidates for use in tissue engineering applications and ideal models for developing, multifunctional structures for nano-technological applications.

Acknowledgements

This work was supported (MG, HF, CT, MS) mainly by the National Science Foundation through the Genetically Engineered Materials Science & Engineering Center (GEMSEC), an MRSEC at UW and partially by NSF-NIRT. This work was also supported (MB, JPS) by funding from the NIDCR-NIH grant, R01 DE01638601. We acknowledge the cell lines provided by Martha Somerman (UW-Periodontics).

Appendix. Supplementary data

The Supplementary data associated with this article can be found in the on-line version at doi:10.1016/j.biomaterials.2010.06.010.

Appendix

Figures with essential color discrimination. Figs. 1, 6, and 7 in this article are difficult to interpret in black and white. The full color images can be found in the on-line version, at doi:10.1016/j.biomaterials.2010.06.010.

References

[1] Yaszemski MJ, Payne RG, Hayes WC, Langer R, Mikos AG. Evolution of bone transplantation: molecular, cellular and tissue strategies to engineer human bone. Biomaterials 1996;17:175–85.
[2] Buck BE, Malinin TI, Brown MD. Bone transplantation and human immunodeficiency virus: an estimate of risk of Acquired Immunodeficiency Syndrome (AIDS). Clin Orth Relat Res 1989;240:129–36.
[3] Stevenson S. Enhancement of fracture healing with autogenous and allogeneic bone grafts. Clin Orth Relat Res 1998;355:S239–46.
[4] Madihally SV, Matthew HWT. Porous chitosan scaffolds for tissue engineering. Biomaterials 1999;20:1133–42.
[5] Bet MR, Goissis G, Vargas S, Selistre-de-Araujo HS. Cell adhesion and cytotoxicity studies over polyanionic collagen surfaces with variable negative charge and wettability. Biomaterials 2003;24:131–7.
[6] Holmes RE. Bone regeneration within a coralline hydroxyapatite implant. Plast Reconstr Surg 1979;63:626–33.
[7] Vacanti CA, Bonassar LJ, Vacanti MP, Shufflebarger J. Replacement of an avulsed phalanx with tissue-engineered bone. N Engl J Med 2001;344:1511–4.
[8] Yuan HP, Kurashina K, de Bruijn JD, Li YB, de Groot K, Zhang XD. A preliminary study on osteoinduction of two kinds of calcium phosphate ceramics. Biomaterials 1999;20:1799–806.
[9] Flatley TJ, Lynch KL, Benson M. Tissue response to implants of calcium phosphate ceramic in the rabbit spine. Clin Orth Relat Res 1983;179:246–52.
[10] Graves GA, Noyes FR, Villanueva AR. The influence of compositional variations on bone ingrowth of implanted porous calcium aluminate ceramics. J Biomed Mater Res 1975;9:17–22.
[11] Cato TL, Saadiq FE-A, Sobrasua EI, Darryl AW, Mohamed A, Harry RA, et al. A highly porous 3-dimensional polyphosphazene polymer matrix for skeletal tissue regeneration. J Biomed Mater Res 1996;30:133–8.
[12] Dietmar WH, Thorsten S, Iwan Z, Kee Woei N, Swee Hin T, Kim Cheng T. Mechanical properties and cell cultural response of polycaprolactone scaffolds designed and fabricated via fused deposition modeling. J Biomed Mater Res 2001;55:203–16.
[13] Addadi L, Weiner S. Interactions between acidic proteins and crystals: stereochemical requirements in biomineralization. Proc Natl Acad Sci U S A 1985;82:4110–4.
[14] Kim HD, Smith JG, Valentini RF. Bone morphogenetic protein 2-coated porous poly-l-lactic acid scaffolds: release kinetics and induction of pluripotent C3H10T1/2 cells. Tissue Eng 1998;4:35–51.
[15] Lowenstam HA. Minerals formed by organisms. Science 1981;211:1126–31.
[16] Bhatnagar RS, Qian JJ, Wedrychowska A, Sadeghi M, Wu YM, Smith N. Design of biomimetic habitats for tissue engineering with P-15, a synthetic peptide analogue of collagen. Tissue Eng 1999;5:53–65.
[17] Burdick JA, Anseth KS. Photoencapsulation of osteoblasts in injectable RGD-modified PEG hydrogels for bone tissue engineering. Biomaterials 2002;23:4315–23.
[18] Lee SY, Choi JH, Xu ZH. Microbial cell-surface display. Trends Biotechnol 2003;21:45–52.
[19] Smith GP, Petrenko VA. Phage display. Chem Rev 1997;97:391–410.
[20] Sarikaya M, Tamerler C, Jen AKY, Schulten K, Baneyx F. Molecular biomimetics: nanotechnology through biology. Nat Mater 2003;2:577–85.
[21] Naik RR, Stringer SJ, Agarwal G, Jones SE, Stone MO. Biomimetic synthesis and patterning of silver nanoparticles. Nat Mater 2002;1:169–72.
[22] Nam KT, Kim DW, Yoo PJ, Chiang CY, Meethong N, Hammond PT, et al. Virus-enabled synthesis and assembly of nanowires for lithium ion battery electrodes. Science 2006;312:885–8.
[23] Sarikaya M. Biomimetics: materials fabrication through biology. Proc Natl Acad Sci U S A 1999;96:14183–5.
[24] Sarikaya M, Tamerler C, Schwartz DT, Baneyx FO. Materials assembly and formation using engineered polypeptides. Annu Rev Mater Res 2004;34:373–408.
[25] Tamerler C, Khatayevich D, Gungormus M, Kacar T, Oren EE, Hnilova M, et al. Molecular biomimetics: GEPI-Based biological routes to Technology. Biopolymers 2010;94:78–94.
[26] Sano KI, Sasaki H, Shiba K. Specificity and biomineralization activities of Ti-binding peptide-1 (TBP-1). Langmuir 2005;21:3090–5.
[27] Jefferiss CD, Lee AJC, Ling RSM. Thermal aspects of self-curing Polymethylmethacrylate. J Bone Jt Surg Br 1975;57-B:511–8.
[28] Yaszemski MJ, Payne RG, Hayes WC, Langer R, Mikos AG. In vitro degradation of a poly(propylene fumarate)-based composite material. Biomaterials 1996;17:2127–30.
[29] Muggli DS, Burkoth AK, Anseth KS. Crosslinked polyanhydrides for use in orthopedic applications: degradation behavior and mechanics. J Biomed Mater Res 1999;46:271–8.
[30] Alireza SS, Xuezhong H, Esmaiel J. Effect of osteonectin-derived peptide on the viscoelasticity of hydrogel/apatite nanocomposite scaffolds. Biopolymers 2007;85:370–8.
[31] Aulisa L, Dong H, Hartgerink JD. Self-assembly of multidomain peptides: sequence variation allows control over cross-linking and viscoelasticity. Biomacromolecules 2009;10:2694–8.
[32] Cui HG, Webber MJ, Stupp SI. Self-assembly of peptide amphiphiles: from molecules to nanostructures to biomaterials. Biopolymers 2010;94:1–18.
[33] Gao Y, Yang ZM, Kuang Y, Ma ML, Li JY, Zhao F, et al. Enzyme-instructed self-assembly of peptide derivatives to form nanofibers and hydrogels. Biopolymers 2010;94:19–31.
[34] Hosseinkhani H, Hosseinkhani M, Tian F, Kobayashi H, Tabata Y. Bone regeneration on a collagen sponge self-assembled peptide-amphiphile nanofiber hybrid scaffold. Tissue Eng 2007;13:11–9.
[35] Jung JP, Gasiorowski JZ, Collier JH. Fibrillar peptide gels in Biotechnology and Biomedicine. Biopolymers 2010;94:49–59.
[36] Kazunori H, Motohiro H, Toshihiko Y, Hajime O. Spatial distribution of mineralized bone matrix produced by marrow mesenchymal stem cells in self-assembling peptide hydrogel scaffold. J Biomed Mater Res Part A 2008;84A:128–36.
[37] Kisiday J, Jin M, Kurz B, Hung H, Semino C, Zhang S, et al. Self-assembling peptide hydrogel fosters chondrocyte extracellular matrix production and cell division: Implications for cartilage tissue repair. Proc Natl Acad Sci U S A 2002;99:9996–10001.
[38] Kretsinger JK, Haines LA, Ozbas B, Pochan DJ, Schneider JP. Cytocompatibility of self-assembled β-hairpin peptide hydrogel surfaces. Biomaterials 2005;26:5177–86.
[39] Krishna OD, Kiick KL. Protein- and peptide-modified synthetic polymeric biomaterials. Biopolymers 2010;94:32–48.
[40] MacEwan SR, Chilkoti A. Elastin-like polypeptides: biomedical applications of tunable biopolymers. Biopolymers 2010;94:60–77.
[41] Rapaport H, Grisaru H, Silberstein T. Hydrogel scaffolds of amphiphilic and acidic β-sheet peptides. Adv Funct Mater 2008;18:2889–96.
[42] Woolfson DN. Building fibrous biomaterials from alpha-helical and collagen-like coiled-coil peptides. Biopolymers 2010;94:118–27.
[43] Zhan H, Timothy DS, James FH, Alvaro M, Pablo Jr B, Chung-Yan K, et al. Bioactive nanofibers instruct cells to proliferate and differentiate during enamel regeneration. J Bone Miner Res 2008;23:1995–2006.
[44] Nagarkar RP, Schneider JP. Synthesis and primary characterization of self-assembled peptide-based hydrogels. Methods Mol Biol 2008;474:61–77.
[45] Pantoja-Uceda D, Santiveri CM, Jiménez MA. De novo design of monomeric β-hairpin and β-sheet peptides. Methods Mol Biol 2006;340:27–51.
[46] Branco MC, Nettesheim F, Pochan DJ, Schneider JP, Wagner NJ. Fast dynamics of semiflexible chain networks of self-assembled peptides. Biomacromolecules 2009;10:1374–80.

[47] Haines-Butterick L, Rajagopal K, Branco M, Salick D, Rughani R, Pilarz M, et al. Controlling hydrogelation kinetics by peptide design for three-dimensional encapsulation and injectable delivery of cells. Proc Natl Acad Sci 2007;104:7791–6.

[48] Altunbas A, Sharma N, Lamm MS, Yan CQ, Nagarkar RP, Schneider JP, et al. Peptide–silica hybrid networks: biomimetic control of network mechanical behavior. ACS Nano 2009;4:181–8.

[49] Hule RA, Nagarkar RP, Altunbas A, Ramay HR, Branco MC, Schneider JP, et al. Correlations between structure, material properties and bioproperties in self-assembled beta-hairpin peptide hydrogels. Faraday Discuss 2008;139:251–64.

[50] Gungormus M, Fong H, Kim IW, Evans JS, Tamerler C, Sarikaya M. Regulation of in vitro calcium phosphate mineralization by combinatorially selected hydroxyapatite-binding peptides. Biomacromolecules 2008;9:966–73.